Supplementary Figure Legends

Figure S1. Validation of the home made NET ELISA assay. A. To examine the sensitivity of the NETs ELISA, we treated isolated human neutrophils with increasing PMA concentrations (0.1-2 μM) for 4 hours at 37˚C to induce NETosis and obtained a dose-dependent response, which was lost in the presence of DNase1 (400 units/mL) ($p=0.036$ and $p=0.029$ for a PMA concentration of 1 μM and 2 μM, respectively). **B**. Dot plot of isolated human neutrophils that are stimulated or not with PMA (2 μM) for 4 hours at 37˚C (from panel A) and stained with Sytox Orange to assess NET levels *in vitro*. **C**. Fluorescence images of the stimulated and non-stimulated wells stained with Sytox Orange (from panel B) showing NET formation in the presence of PMA. **D**. The NETs ELISA did not detect DNA extracted from neutrophils (PMN DNA) or from several cancer cell lines (human colon L174D, human cervical HELA and human lung A549) while it detected low levels of NETs in unstimulated PMNs and a significant 3-fold increase in PMA-stimulated neutrophils ($p=0.045$). Neutrophils were purified from healthy individuals and 10^6 cells were used for all conditions. **E.** We sought to determine whether the assay could measure NETs in circulation (plasma or serum collected from human whole blood). We observed that stimulating whole blood with 0.5 μM PMA for 1 hour at 37˚C resulted in a significant 3.4-fold increase in NET levels in plasma ($p=0.033$), which was abrogated by pre-treatment with 10 μM NE inhibitor (NEi or Sivelestat) to inhibit NET formation or 400 units/mL DNase1 to degrade NETs ($p=0.033$ and $p=0.034$, respectively). Similar treatment of unstimulated whole blood with DNase1 or NEi also led to significantly lower NET levels ($p=0.001$ and $p=0.027$, respectively).

For all panels: n=3-5, *p < 0.05 as determined using a T-test for panel A and one-way ANOVA for panels D and E.

Figure S2. NET levels correlate with T, N and M stage in the esophagogastric (EGA) and lung (LAC) adenocarcinoma cancer cohorts. A. Normalized NET absorbance of the EGA patients are plotted for patients with clinical T1-T2 tumors (n=7) and T3-T4 tumors (n=30). **B.** Normalized NET absorbance of the EGA patients are plotted for patients with clinical N- (n=14) and N+ (n=23). **C.** Normalized NET absorbance of the EGA patients are plotted for patients with M0 (n=29) and M1 (n=8). **D.** Normalized NET absorbance of the LAC patients are plotted for patients with clinical T stage 1 (n=9) and T stage 2+ (n=14). For all panels, mean ± SEM of each group is shown along with respective p values determined using T-test and one-way ANOVA.

Figure S3. Circulating NET levels are a better predictor of tumor progression than neutrophil to lymphocyte ratio (NLR) in EGA and LAC patients. A. NLRs of the EGA patients are plotted for patients with overall clinical stages I-II (n=12) and III-IV (n=25). **B.** NLRs of the EGA patients are plotted for patients with clinical T1-T2 tumors (n=7) and T3-T4 tumors (n=30). **C.** NLRs of the LAC patients are plotted for patients with overall pathological stage I (n=16) and II-III (n=8). **D.** NLRs of the LAC patients are plotted for patients with pathological T1 tumors (n=9) and T2-T3 tumors (n=14). For panels A-D, mean ± SEM of each group is shown. **E.** Correlation analysis is performed on NET absorbance and NLR in the EGA and LAC cohorts combined. For all panels p values are shown as determined using a T-test.

Figure S4. Circulating NET levels are a better predictor of tumor progression than absolute neutrophil count in EGA and LAC patients. A. Absolute neutrophil counts of the EGA patients are plotted for patients with overall clinical stages I-II (n=12) and III-IV (n=25). **B.** Absolute neutrophil counts of the EGA patients are plotted for patients with clinical T1-T2 tumors (n=7) and T3-T4 tumors (n=30). **C.** Absolute neutrophil counts of the LAC patients are plotted for patients with overall pathological stage I (n=16) and II-III (n=8). **D.** Absolute neutrophil counts of the LAC patients are plotted for patients with pathological T1 tumors (n=9) and T2-T3 tumors (n=14). For panels A-D, mean ± SEM of each group is shown. **E.** Correlation analysis is performed on NET absorbance and absolute neutrophil count in the EGA and LAC cohorts combined. **F.** Correlation analysis is performed on NLR and absolute neutrophil count in the EGA and LAC cohorts combined. For all panels p values are shown as determined using a T-test.

Figure S5. Image Flow Cytometry as a tool to measure NETosis. A. Representative images of neutrophils isolated from the peripheral blood of non-tumor bearing C57BL/6 mice unstimulated or stimulated with 0.5 μM PMA for 4 hours and stained with DAPI (red) and Ly6G-1A8 (green). A merge image is also presented (orange). **B.** Raw data of the image flow cytometry experiments showing the population selected in the analysis to measure single cell neutrophil's nuclear area. Channel 1 (ch01): bright-field; channel 2 (ch02): FITC; Channel 7 (ch07): DAPI.

Figure S6. Flow cytometry as a tool to measure lung metastasis. Representative flow cytometry graphs of H59-GFP cells extracted from the lungs of tumor-bearing mice (TBM) for the four conditions used in Figure 5.

Figure S7. Tumor-bearing mice (TBM) do not have massive NET deposition in metastatic organs. A. Shown are western blots performed on cell lysates of tissue homogenates (primary flank tumor as well as liver and lung metastatic tissues) from 3 C57BL/6 TBM probing for H3Citrulline (and β-actin as a loading control). **B.** Representative images of multiplex IF performed on FFPE lung and livers extracted from C57BL/6 TBM probing for Ly6G (green) and H3Cit (red). Scale = 50 μm.

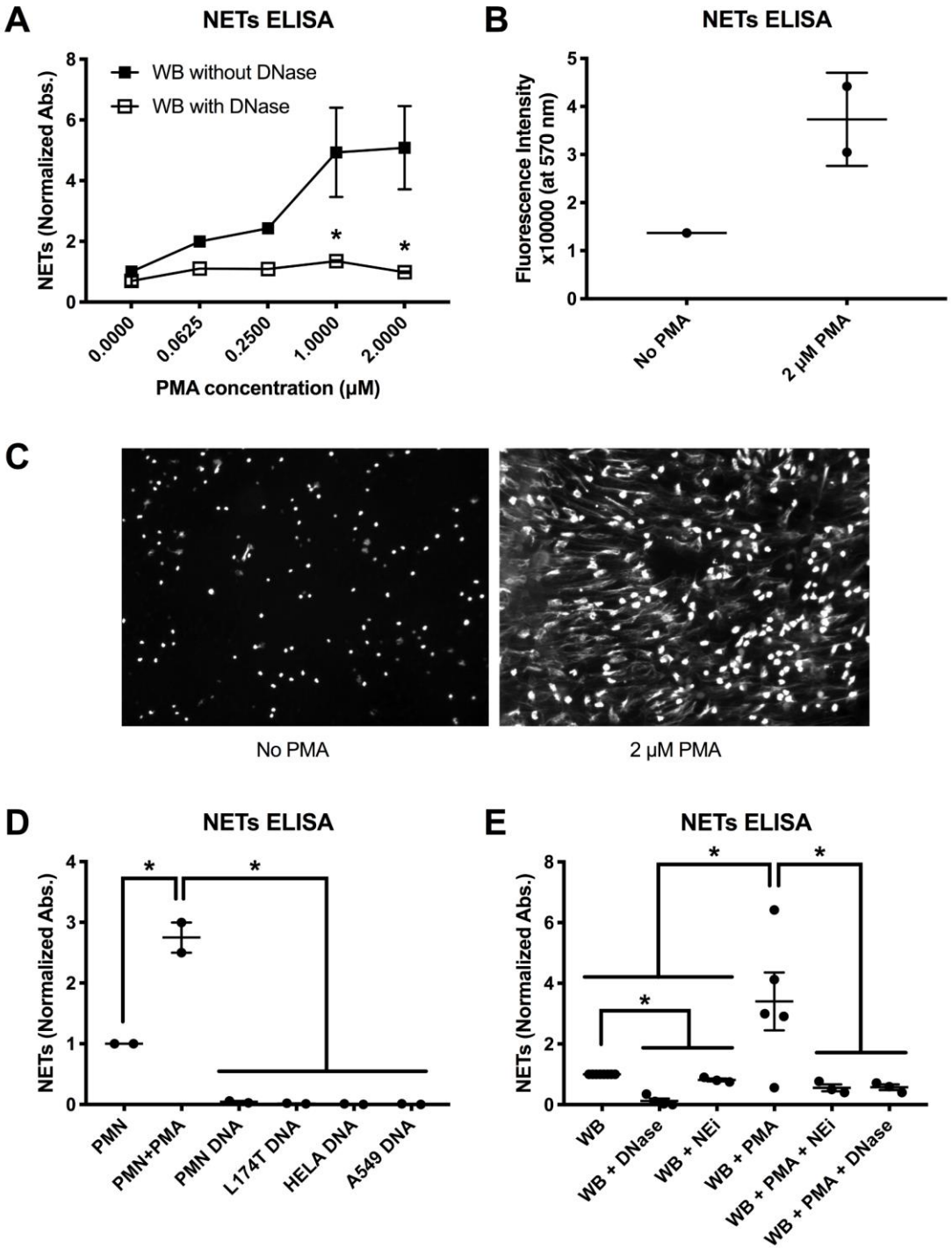

Supplementary Figure 1

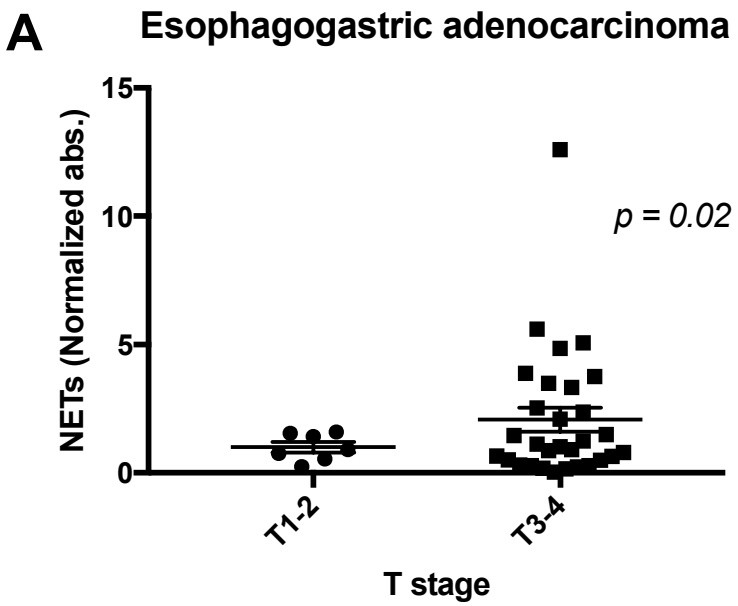

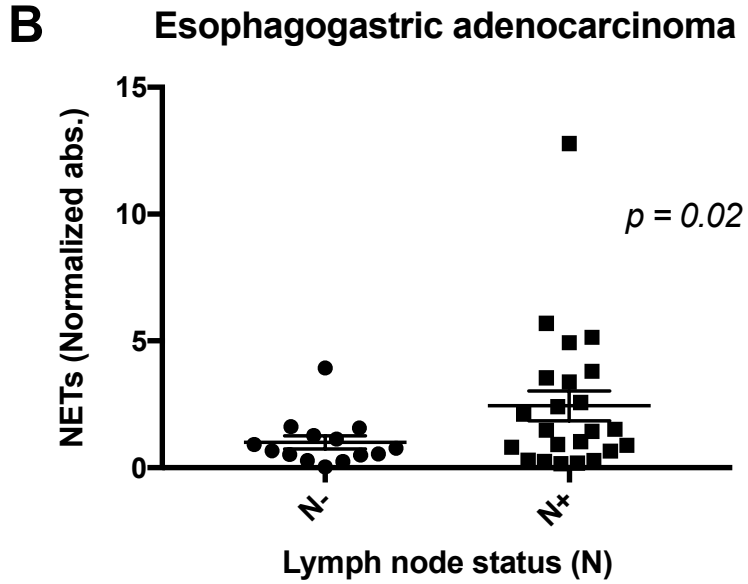

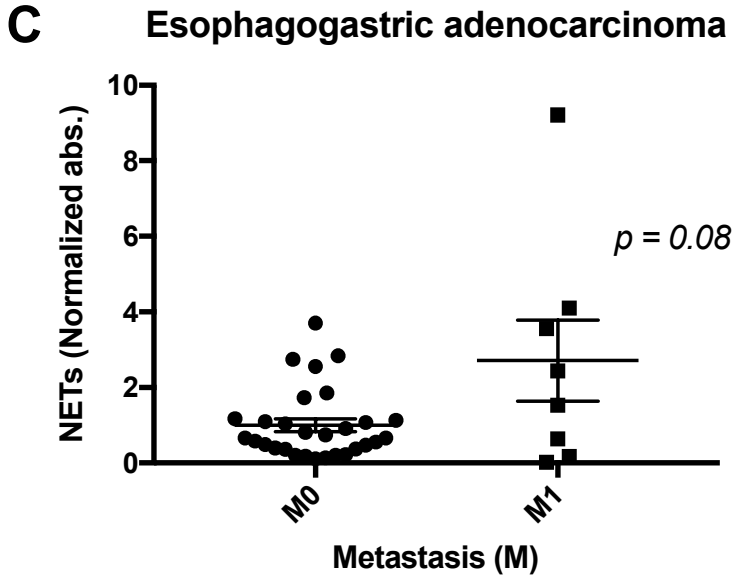

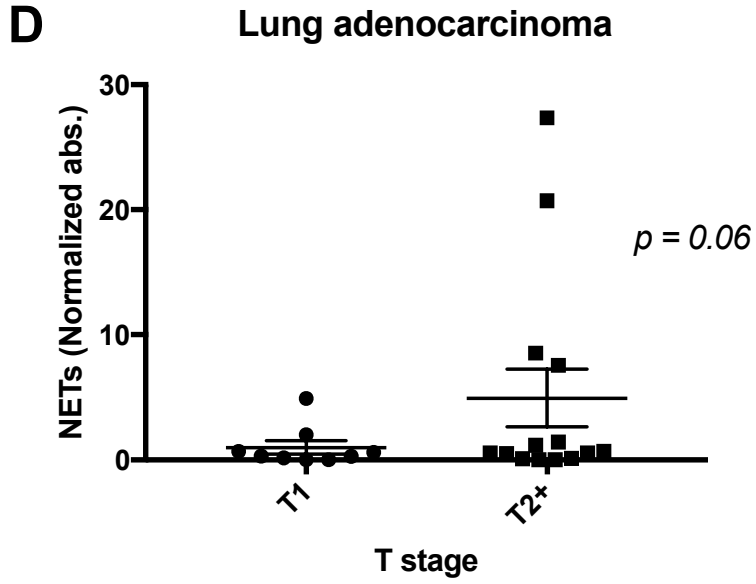

Supplementary Figure 2

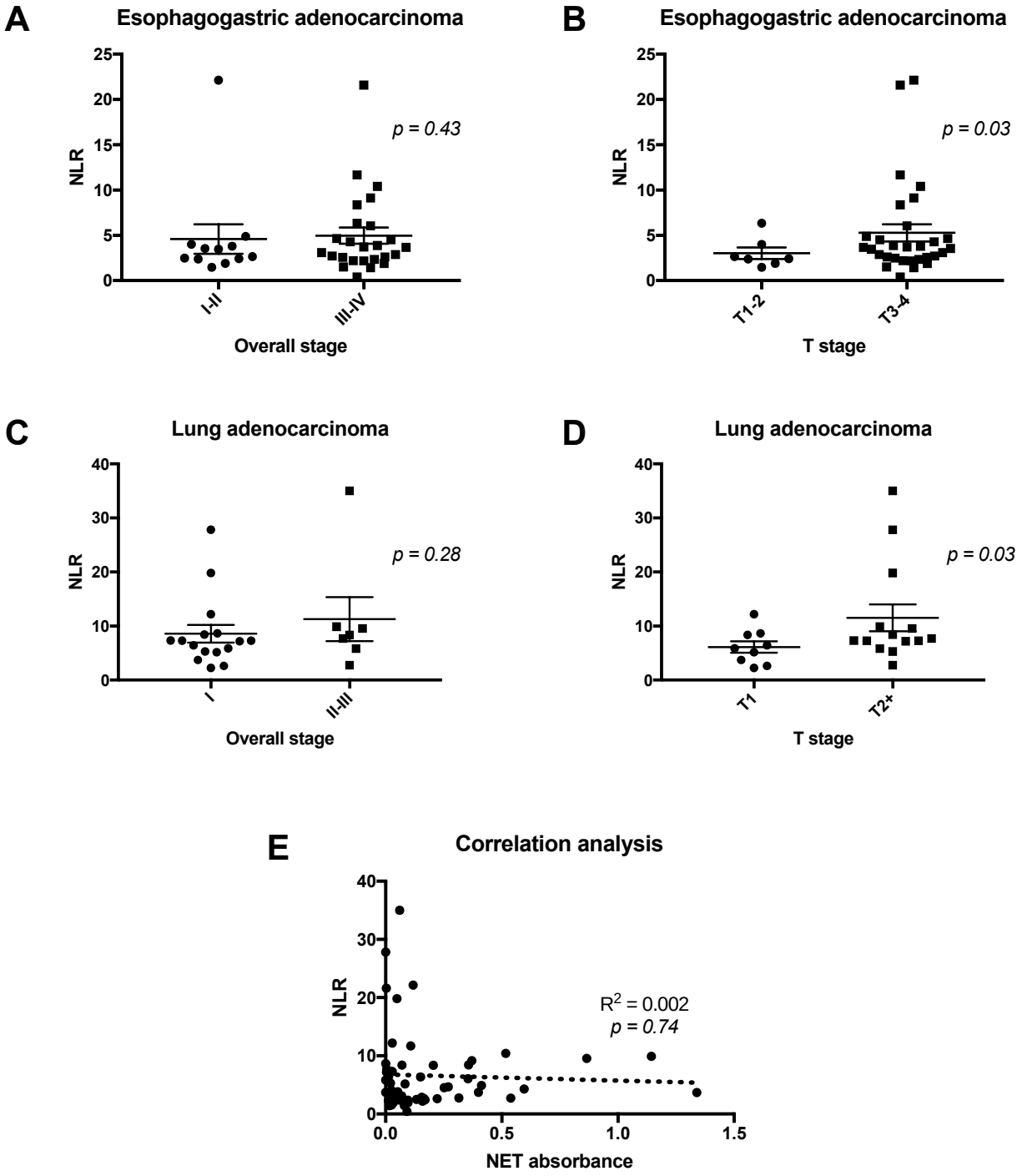

Supplementary Figure 3

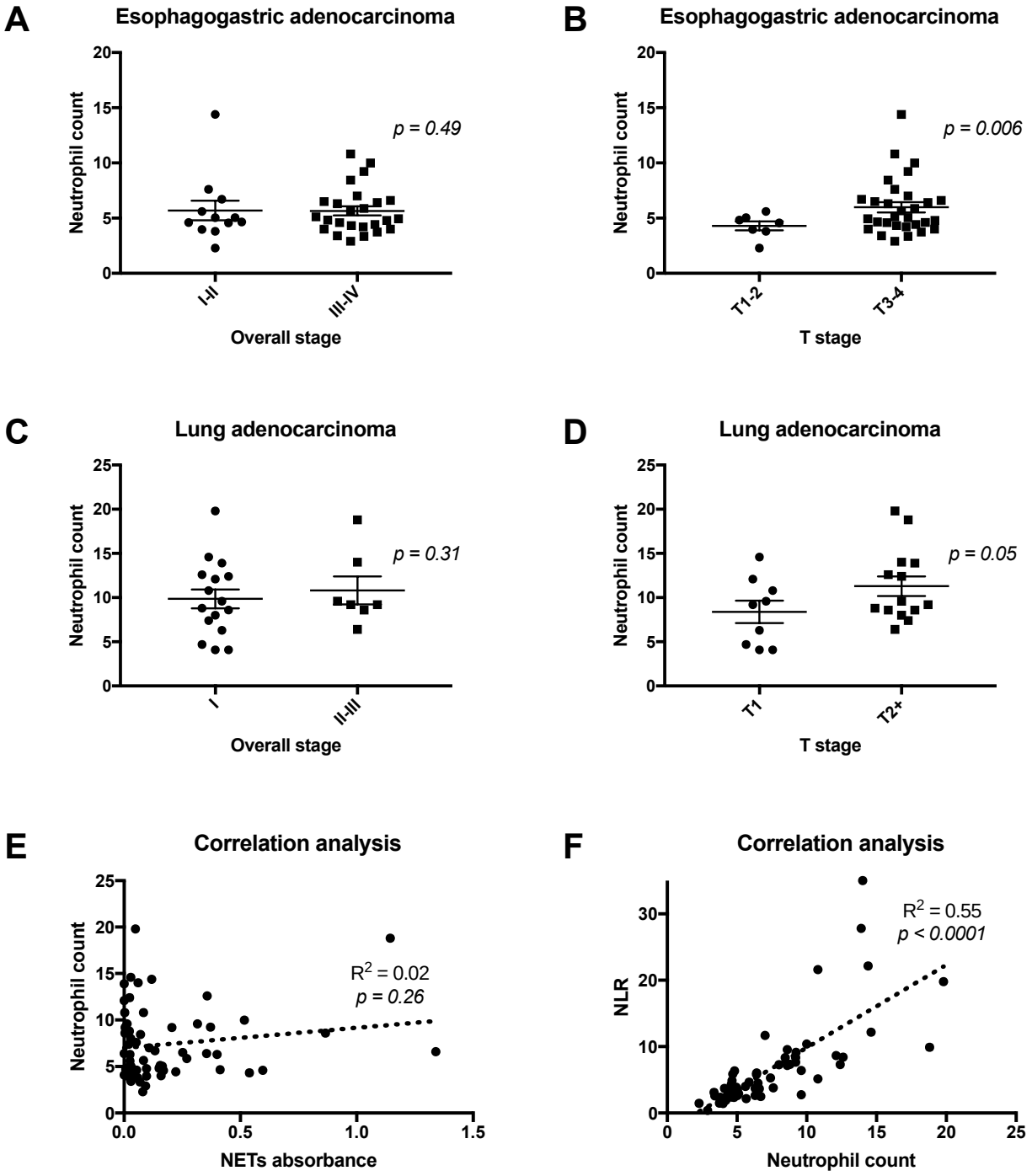

Supplementary Figure 4

A

B

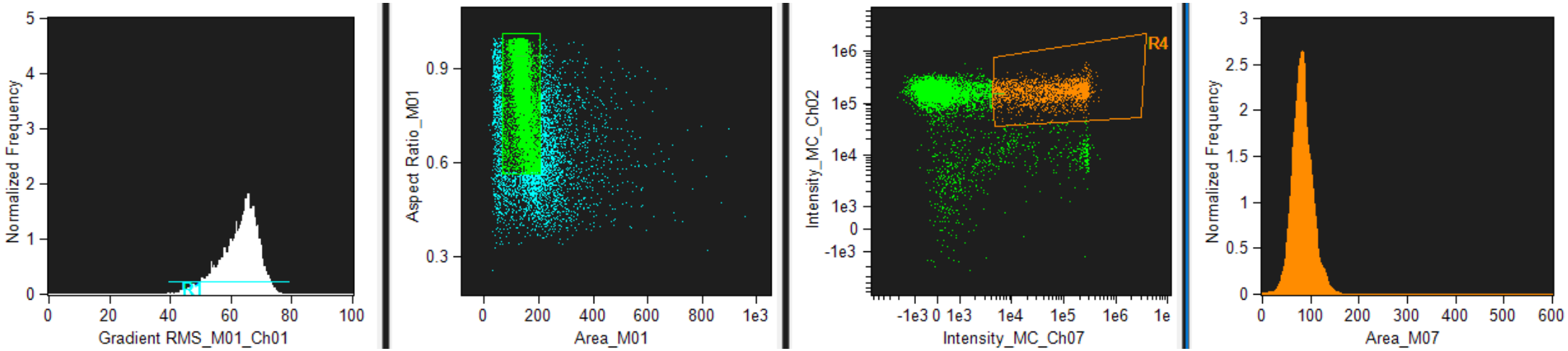

Supplementary Figure 5

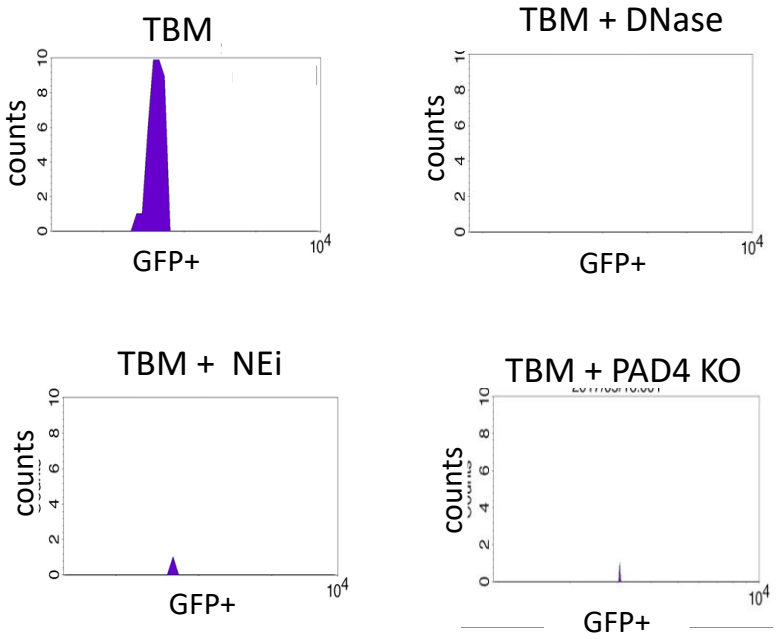

Supplementary Figure 6

A

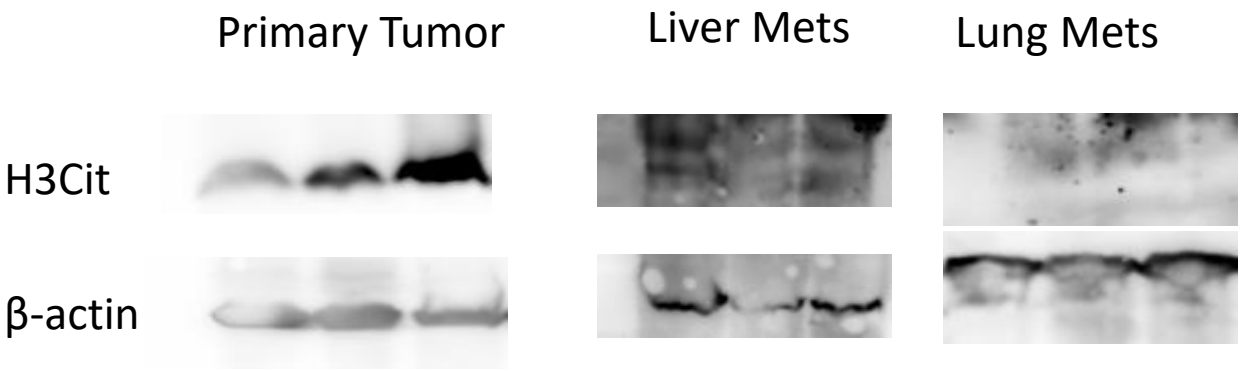

B

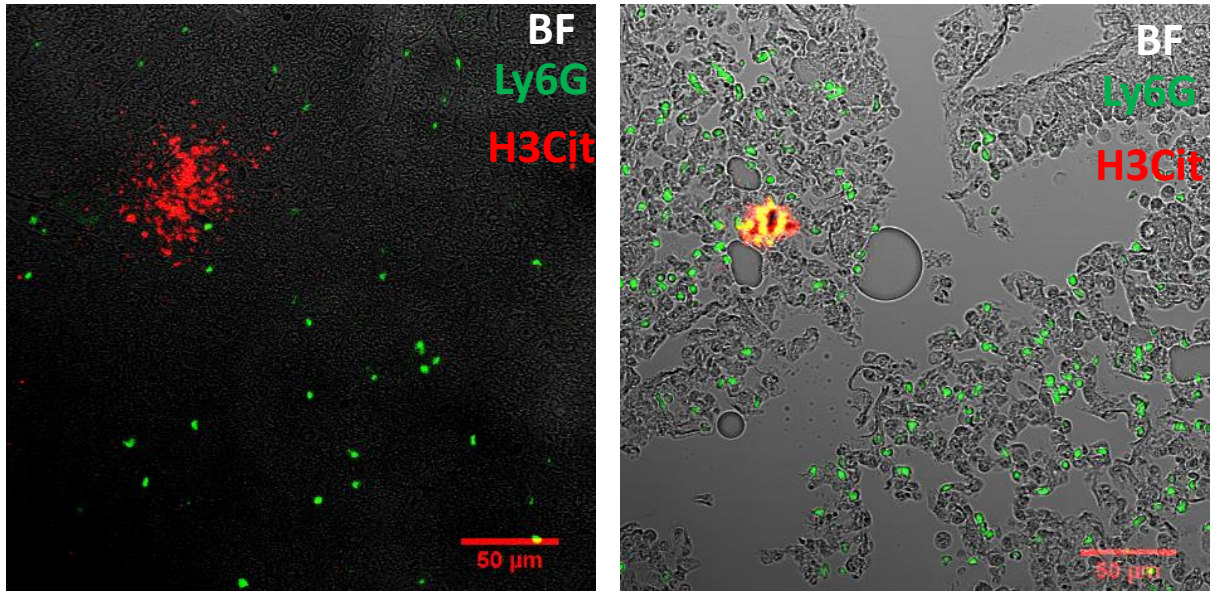

LIVER

LUNG

Supplementary Figure 7